Influence of Si content on the machinability of ductile iron

Tiago Silvério Guimarães Xavier [1] ⓘ
Leonardo Rosa Ribeiro da Silva [1,2*] ⓘ
Wilson Luiz Guesser [3,4†] ⓘ
Alisson Rocha Machado [1,2] ⓘ

Abstract

The development of new chemical compositions of cast iron contributes to increasing the competitiveness of foundry and manufacturing companies that always seek to optimize the properties of these materials. Previous works detected machinability variation along the cross-section of nodular cast irons (DI) bars produced by continuous casting due to the variation of the microstructure and mechanical properties presented, with decreasing machinability from the periphery to the core. This variation imposes complications, as it implies different ideal (or optimal) cutting conditions along the cross-section of the round bars. Assays with ductile irons (DI) with varying silicon content showed that the reduction in silicon decreased the microhardness of ferrite and increased the percentage of pearlite in the matrix, thus generating a decrease in the ductility of the material. Thus, this work investigates the effect of silicon content on machinability variation along the cross-section of nodular cast iron bars in the turning process. Three different types of nodular cast iron alloys were used, differing by the amount of silicon in the composition. Material characterization and machining tests were carried out in three regions: the periphery, the intermediate region, and the core. The hardness, metallography, size of graphite nodules, and amount per region were analyzed in the characterization tests and compared to the evolution of wear and tool life machining force and surface roughness. The addition of different percentages of silicon did not avoid the differences in behavior between the three regions of the same material, but it changed the behavior of the three alloys studied. The silicon content affects the material's microstructure, which, together with the cooling rate, favors the differentiation of graphite nodules in different sizes, arrangements, and spacing. This differentiation contributes to the difference in the material's behavior in the machining between the regions along the cross-section. Strengthening in the core region was a trend in all three alloys. There was a statistical difference in roughness between the regions of the material. Cast iron with medium silicon content showed lower machining force and roughness values but close to those of high silicon. As with high-silicon cast iron, the forces remained at a more stabilized level, without significant variations between regions of the material.

Keywords: Nodular cast iron; Machinability; Silicon content; Turning; Tool life; Machining force; Surface finish.

1 Introduction

According to Guesser [1], the development of new chemical compositions of cast iron, optimizing its properties, contributes to greater competitiveness of foundry and manufacturing companies. As virtually all castings undergo machining, this process becomes vital in improving alloys. Factors that influence the properties of cast iron include the chemical composition of the matrix and the size, distribution, volume fraction, and morphology of the individual components of the microstructure. There is extensive literature on the influence of microstructure on the mechanical properties of ductile alloy cast irons [2].

The crystallization of graphite nodules in cast iron is initiated by compounds acting as heterogeneous nuclei. Sulfur promotes precipitation of such non-metallic substrates, increasing the nodule count [3]. Applications of cast irons, from mundane to more challenging, are decided by the morphology of free graphite in the metallic matrix [4].

In the continuous casting process (FUCO) [5], bars with large cross-sections are produced, with varying mechanical and metallurgical properties along the section, caused by different cooling rates from the periphery to the core. This process represents an exciting alternative for manufacturing cast iron parts, producing profiles with different section formats. Different grades of gray and nodular cast iron are manufactured through this process. The parts produced by these products are gears, crankshafts, molds for glassware, hydraulic controls, hydraulic pistons, bushings, pulleys, bearing covers, and various parts for maintenance.

[1]Faculdade de Engenharia Mecânica, Universidade Federal de Uberlândia, UFU, Uberlândia, MG, Brasil.
[2]Pontifícia Universidade Católica do Paraná, PUC-PR, Curitiba, PR, Brasil.
[3]Centro de Ciências Tecnológicas, Universidade do Estado de Santa Catarina, UDESC, Joinville, SC, Brasil.
[4]Rua Albano Schmidt, 3400, Zi Tupy, Joinville - SC, 89206-101, Brasil
[†]In memoriam

*Corresponding author: leonardo.rrs@gmail.com

The continuous casting process (FUCO) [5] has the main advantage of optimizing production and increasing bar volume. Figure 1 shows the diagram of the bar manufacturing process by continuous casting. In this process, the molten material (1) is deposited in the filling spout (2) to supply the process feed. Due to its high thermal conductivity, the graphite mold contributes to high heat extraction from the liquid iron during casting. As a result of the high heat extraction, a shell is formed on the material in contact with the mold (4); however, the core remains in the liquid phase. This mold receives water inside to exchange heat, contributing to the solidification process of the bar. The inlet and outlet of water are represented in the figure in item (11). The bar is cooled by the air when pulled out of the shell by a set of rollers (7).

During the solidification of the bar, a temperature gradient appears along the cross-section. As a result of this temperature gradient, property differences arise between the bar's periphery and core, causing differences in machinability, as evidenced by the master's work by Ângelo [6] and PhD work by Sousa [7]. This implies the need to adopt different cutting conditions along the radius of the part since each region presents different ideal conditions. For this reason, foundry companies seek a chemical composition and microstructure that ensure more homogeneous properties, reducing this variability in machining behavior along the cross-section of the bars. One of the possibilities is to look for an ideal silicon content.

After solidification is complete, further cooling in the solid-state results in decreased dissolved carbon content in the austenite, which precipitates onto existing graphite particles [1]. Also, according to Guesser [1], irons Silicon and molybdenum alloyed castings represent an essential family of cast irons specially designed for hot work. Increasing the Si content increases the ferrite/austenite transformation temperature, thus increasing the field of utilization of the ferritic matrix component. This characteristic is essential because the ferritic field is expanded instead of increasing the stability of pearlite with alloying elements. Ferrite has low strength and, to compensate for this effect, high levels of silicon are used (usually 1.0 – 3.0%, reaching 5.5%), promoting the hardening of the solid solution and molybdenum (0.3 – 1.0%), an element that promotes hot hardening. It also increases resistance to oxidation [1]. Another characteristic of silicon is that it is graphitizing. When present in cast iron alloys, this characteristic accelerates cementite decomposition, forming graphite.

According to Stan et al. [8], silicon is the most representative element in the composition of cast iron, with an essential role in the solidification process and graphitizing effect. Silicon inoculation is vital in the transition from liquid to solid state in cast iron, contributing to achieving high ductility and toughness characteristics with better machinability conditions.

According to these authors, ductile cast irons with 2.5–3.5% Si are more sensitive to high solidification temperature subcooling (but with a higher inoculation efficiency) than cast irons containing 4.5–5.5% Si in a lower subcooling level (but also a lower inoculation effect). In high Si nodular cast iron (above 4.0% Si), the main objective of inoculation is

1. Liquid metal
2. Filling spout
3. Microwave power
4. Graphite water cooled mold
5. Support rollers
6. Control panel
7. Tractor unit
8. Cutting unit
9. Broken drive
10. Cut bar – FUCO
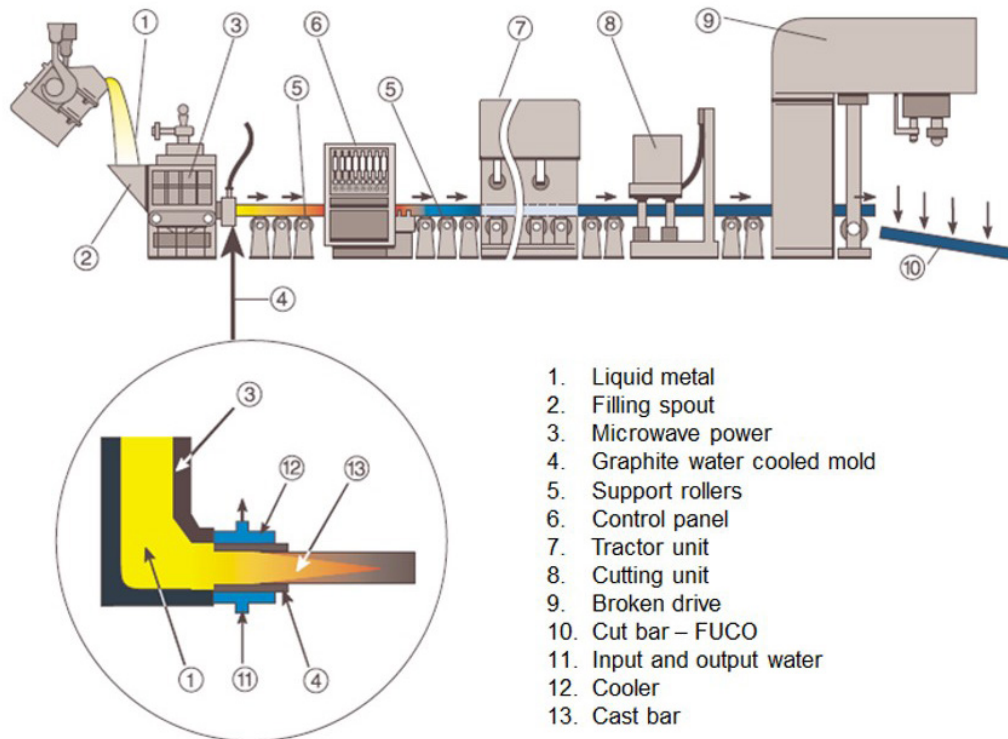11. Input and output water
12. Cooler
13. Cast bar

Figure 1. Continuous casting process [5].

not to avoid carbides but rather to improve the degree of nodular compaction of the graphite affected by Si.

Another characteristic of silicon is that it is graphitizing. This characteristic makes this element in cast iron alloys accelerate cementite decomposition, forming graphite. According to Vilela et al. [9], the cooling speed of cast iron influences the amount of ferrite in the microstructure, consequently its behavior in relation to mechanical properties. Higher cooling speed reflects in shorter residence time at stable and metastable eutectoid temperatures, resulting in a lower percentage of ferrite in the matrix.

According to Guesser [1], as a rule, as the Si content increases in nodular cast iron, its strength limit increases, and therefore there is a decrease in machinability. Nodular cast iron has more excellent resistance to chip breaking than gray cast iron, with longer contact time between chip and tool, accentuating tool wear mechanisms. Guesser [1] concluded that the hardening of ferrite due to silicon in cast iron produced by continuous casting causes an increase in tool wear in turning.

For Arshad et al. [10], the silicon content increased the elongation of graphite nodules to a certain extent and reduced the tensile strength. The increase in silicon content up to 2.8% generated a decrease in the ferrite content and reduced tensile strength. After this value, silicon strengthens the ferrite, thus increasing the mechanical strength of the microstructure. It was concluded that the tensile strength decreased for silicon values above 2.8%. A further increase in silicon content led to an increase in tensile strength and yield strength. Hardness gradually decreased as silicon content was increased, and the variation in hardness at different points decreased as ferritic ductile iron was reached.

Martins [11] studied the influence of silicon content in nodular cast irons in the drilling process and concluded that the best machinability among the materials studied was with medium silicon content, considering the cutting efforts. The lower percentage of pearlite justified this conclusion compared to material with low silicon content and the lower hardness of ferrite compared to material with the high silicon content.

Therefore, this work proposes to investigate the machinability along the cross-section of three nodular cast irons produced by continuous casting with different silicon contents to identify the one that best distributes the properties along the cross-section and, consequently, the machinability.

2 Experimental procedure

The present work used the nodular cast iron NBR FE-45012 with different silicon contents. The materials were characterized metallographically and by hardness tests and tested in the turning process, considering the machining force, tool life, and workpiece roughness. The wear mechanisms of the tools after the life tests were also analyzed.

2.1 Machined materials

The material used for the tests in this work were NBR FE-45012 nodular cast iron bars produced by continuous casting. Three versions of this material were tested, with low, medium, and high silicon contents. The three versions of the material, high, medium, and low silicon content have the compositions indicated in Table 1, according to data provided by the manufacturer, TUPY S.A.

The mechanical and metallurgical properties of the materials, stratified by region (core - NU, half radius - MR, and periphery - PE), are shown in Table 2, provided by TUPY S.A. The materials were supplied in cylindrical bars of 500 mm in length and, after being cleaned (peeled), had a diameter of 88 mm. Martins [11] named the three compositions high, medium, and low silicon. The material belongs to class FE-45012 and has the compositions indicated in Table 2 and supplied by TUPY. TUPY provided the material properties shown in Table 2 with the metallurgical properties of the different regions.

The material was divided into three distinct regions: periphery, intermediate zone, and core, keeping the same area per region to carry out the experiments. An area in the center of the bars was discounted, with a diameter of 30 mm, minimum final diameter limit of the machined bar, to maintain sufficient material volume inside the sample to avoid system vibration during machining, maintain the rigidity of the assembly, even in the more severe machining conditions. This central region also serves to fit the counterpoint of the vise for a good fixation of the bar in the lathe.

Figure 2 illustrates the bar's cross-section, identifying the three regions for characterization and testing. From the radius of 44.00 mm to the radius of 36.96 mm, the area in blue was called the periphery.

With a radius varying from 36.96 mm to 28.21 mm, the yellow area was called the intermediate zone or simply

Table 1. Chemical composition of the three versions of the NBR FE45012 nodulaar cast iron, according to the manufacturer
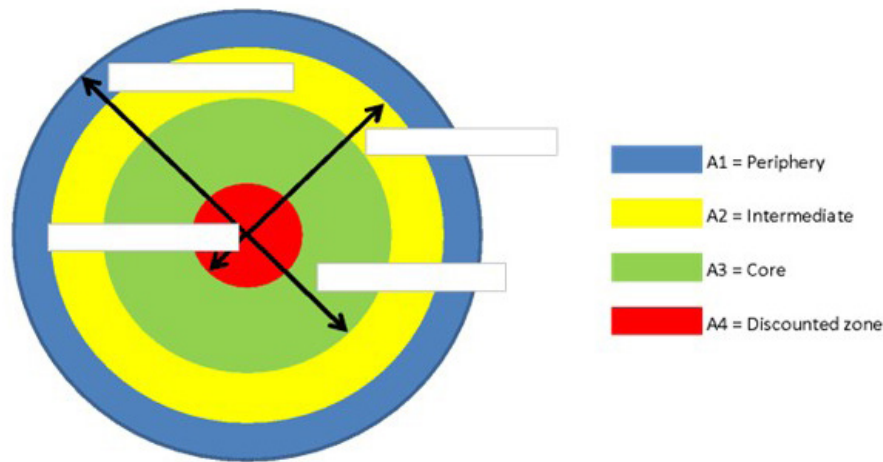
Sample	C	Si	Mn	P	S	Cr	Ti	Sn	Cu	Mg	Ce	Sb
Low Si	3.47	2.52	0.17	0.072	0.008	0.044	0.009	0.004	0.044	0.036	0.0032	0.0005
		2.54										
Medium Si	3.48	3.08	0.18	0.073	0.01	0.047	0.011	0.005	0.046	0.047	0.0065	0.0005
		3.05										
High Si	3.51	4.04	0.16	0.07	0.009	0.045	0.011	0.006	0.039	0.040	0.005	0.0005
		3.92										

Source: TUPY S.A. [12]

Table 2. Mechanical and metallurgical properties of the work materials along their cross-section, according to the manufacturer

Material/Region		Perlite Content [%] Size	Nodular Graphite Nodules/mm²	Ferrite	HV Microhardness (0.05)	Brinell Hardness
126	NU	44	6-7	166	191 ± 10	191 ± 10
	MR	45	6-7	183	190 ± 10	192 ± 10
	PE	15	7-8 (6)	462	188 ± 9	180 ± 9
131	NU	19	6-7-5	178	224 ± 11	173 ± 9
	MR	23	6-7	183	227 ± 11	195 ± 10
	PE	3	7-8	507	231 ± 12	186 ± 9
135	NU	5	6-7	252	278 ± 14	203 ± 10
	MR	7	6-7-5	232	275 ± 14	207 ± 10
	PE	0	7-8 (6)	617	262 ± 14	201 ± 10

Source: TUPY S.A. [12]

Figure 2. Identification of the periphery, intermediate zone, and core of the cross-section of the workpiece bars

intermediate. The area in green, with a radius of 28.21 mm to 15.00 mm, was called the core. These regions have areas of approximately 1790.58 mm². The area in red is the central region of the bar that was not machined, used for fixing the lathe's tailstock.

Two strategies were used to determine the cross-section hardness profile: measurement in 5 random points per region (Figure 3A) and 10 sequential points, starting from the edge, with 3 mm between them (Figure 3B).

Brinell hardness tests were carried out in accordance with the ISO 6507-1 of 2008, using a sphere with a diameter of 2.5 mm and a load of 187.5 kgf. After application, the load was maintained for approximately 30 seconds for all indentations. This precaution was taken, following guidelines from the work of Sousa [13]. The tests were performed on a Wolpert Universal Durometer.

The same samples used in the hardness tests were used for the metallographic analysis. They were cut by a water jet to avoid possible thermal damage. After cutting and hardness tests, the samples were prepared with water-to-metal sandpaper in particle sizes #80, #100, #180, #320, #500, and #1200 mesh, following Pace Technologies [14]. After sanding, they were polished with 3 μm diamond pastes and etched with 2% Nital reagent for 5 seconds, as recommended by Tan and Ögel [15]. The photographs were acquired with

a SONY cyber-shot camera, and the photomicrographs were taken on a Shimadzu microdurometer coupled to a computer. Figures 4 to 6 show the microstructures recorded for materials with low, medium, and high percentages of silicon, also identified by the region of the material photographed.

It is observed that materials with low and medium silicon have similar characteristics when comparing the same regions between the materials and that there are significant differences for the material with high silicon. There are not large amounts of pearlite in this material's intermediate zone and core, as in the other samples. The types of structures found in the materials, regarding the presence of perlite, ferrite, and other constituents, are shown in Table 3.

2.2 Tool life trials

The life and strength tests were carried out in a ROMI CNC lathe, model Multiplic 35D, with 9 kW power and a maximum rotation of 3000 rpm. Following ISO 3685 standard recommendations, average flank wear of 0.3 mm was used as a tool end-of-life criterion. The work methodology consists of machining each material (high, medium, and low silicon), within each region (periphery, intermediate, and core), with a new tool, making several passes until the tool's end-of-life criterion is hit.
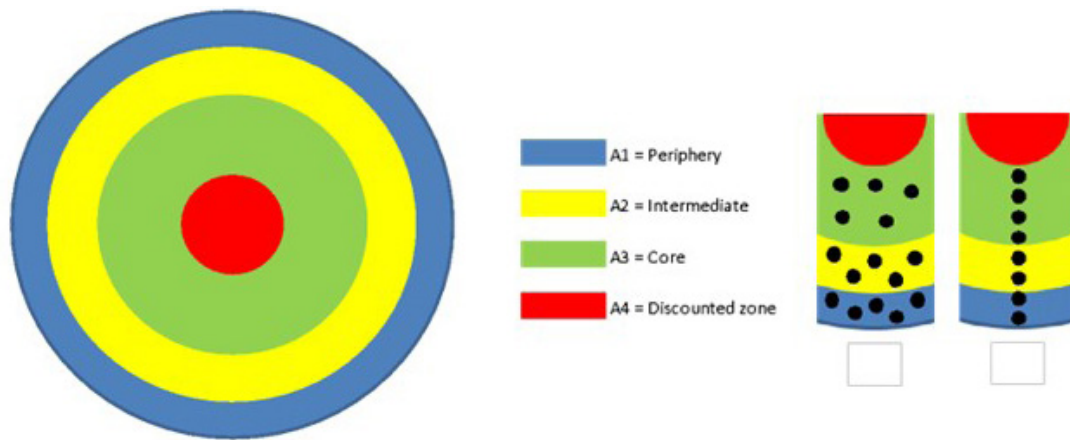
Figure 3. Strategies for measuring the hardness of the cross-section of the bars
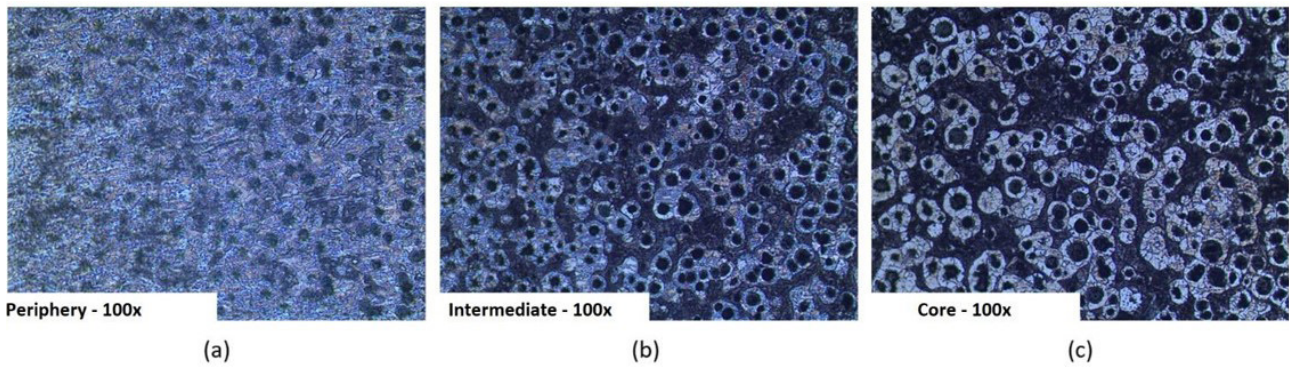

Figure 4. Microstructures of the nodular cast iron with low silicon content; (a) periphery, (b) intermediate zone; (c) core.
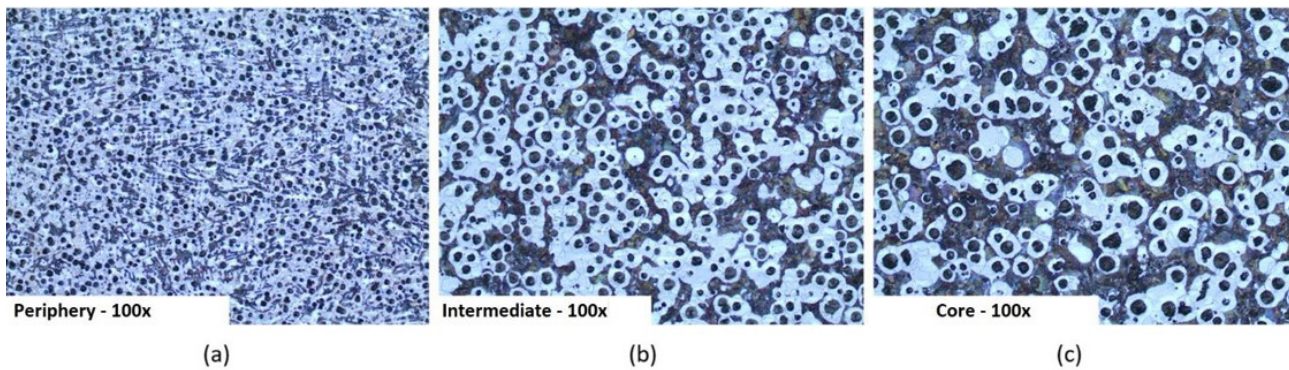

Figure 5. Microstructures of the nodular cast iron with medium silicon content; (a) periphery, (b) intermediate zone; (c) core.
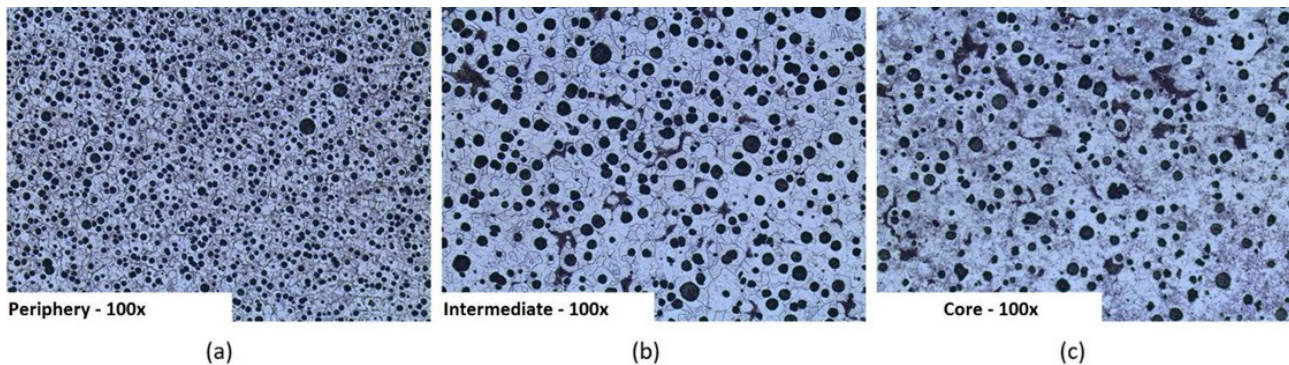

Figure 6. Microstructures of the nodular cast iron with high silicon content; (a) periphery, (b) intermediate zone; (c) core.

Table 3. Microstructures of the work materials

Material	Regions		
	Periphery	Intermediate zone	Core
Low Silicon	Small graphite nodules with pearlite veins and ferritic matrix	Higher graphites and ferrite/pearlite matrix	Higher graphites and ferrite/pearlite matrix
Medium Silicon	Small graphite nodules with pearlite veins and ferritic matrix	Larger graphites and ferrite/pearlite matrix	Larger graphites and ferrite/pearlite matrix
High Silicon	Small graphite nodules with pearlite veins and ferritic matrix	Larger graphites and predominantly ferritic matrix	Larger graphites and predominantly ferritic matrix

Tools from the supplier Tungaloy were used for turning the material tested, with ISO designation SNMA120408, code T5115. It is a square insert with eight cutting edges, without a chip breaker, with a negative rake angle, recommended for finishing and medium cuts. Tools are made of K15 grade carbide, TiN coated.

The roughness parameter Ra was measured during the tool life tests with a Taylor Hobson model S100 Series roughness meter, using a sampling length (cut-off) of 0.8 mm. Three roughness measurements were taken at each tool pass (at each feed path) until the end of the tool life. The average of each pass was calculated, and then the global average for each material region.

For the tool life tests, a $2*3^2$ factorial design was used.

The planning decision is to keep the feed (0.4 mm/rev) and to cut depth (1.0 mm) constant, with process variables being the material and the tool's region, material, and cutting speed. Initially, it was thought to treat all variables as quantitative, but this would only be possible if the material characteristics along the cross-section were guaranteed to be fixed. The metallographic analysis noticed differences in the microstructure; the material and material region variables were qualitative in the planning. The cutting speed values were chosen based on pre-tests so that the tool life can be statistically compared. The representation of the variables is in Table 4.

The Factorial Planning had a variable with two levels (cutting speed) and two variables with three levels (material and material region), as shown in Table 3. Filtering the planning, there is a total of 18 tests. Due to the limited material available, only one repetition was performed per trial, totaling 36 life trials. At the end of the tests, the wear mechanisms of the tools were analyzed in the scanning electron microscope (SEM) Hitachi TM3000.

2.3 Cutting force trials

For the cutting forces tests, a Kistler® model 9265B dynamometer was used, with a Kistler amplifier, model 5019A. The specific tests (cutting forces and roughness) of the turning were carried out on 220 mm long bars, one of each different composition. For data analysis, three points per area were defined (A1, A2, and A3 – mean radius of each region). In these tests, a new edge was used every time the maximum flank wear reached the value of 0.1 mm to avoid the influence of tool wear.

Table 4. Input variables for the tool life tests

Variable type	Process variables	
Qualitative	Work materials	Low Si
		Medium Si
		High Si
	Material regions	Periphery
		Intermediate zone
		Core
Quantitative	Cutting speed	250 m/min
		350 m/min

The depth of cut was kept constant at 1.0 mm for all tests performed. Tests were performed with 4 different feeds (f) in each material region with low, medium, and high silicon for each cutting speed (Vc) tested. The cutting speed values used were 50; 100; 200; 300 m/min. The feed values used were 0.05; 0.1; 0.2; 0.3mm/rev. These values were chosen to evaluate a wider range of cutting speeds and feed rates and not to coincide with the natural vibration frequencies of the dynamometer/tool assembly. Each test produced a feed path of at least 10 mm to allow measurement of roughness. The three force components were measured throughout the test, with an acquisition rate of 1000Hz.

In the strength tests, the roughness parameter Ra was measured with the same roughness meter, and sampling length was used to measure the life tests' roughness. Three roughness measurements were taken along the bar's perimeter for each strength test, considering the calculated mean.

4 Results and discussions

4.1 Hardness trials

Table 5 shows the hardness measurements along the cross-section of the samples, with the five measurement points randomly within the same region. The mean hardness values and respective standard deviation per material, stratified by region, are represented in the table.

The highest hardness values in materials with the low and medium percentage of silicon area in the core region. The peripheral zone has lower hardness values in these materials but a smaller standard deviation between measurements. In high-silicon cast iron, a material with higher hardness values, there is homogeneity concerning the values of this magnitude, which are close in the three regions and with a

low standard deviation. In this material, the highest mean hardness occurred in the intermediate region of the sample.

Figure 7 shows the hardness values measured at the ten points along the diameter of the cross-section, starting from the outermost point, at a diameter of 44 mm, to an inner point, with a diameter of 17 mm, for the three materials tested. These measurements are in relation to the center of the cylindrical sample. Those values present a good correlation with those reported by the manufacturer.

It is observed that, in general, the material with the highest silicon content, as expected, had the highest hardness values compared to materials with medium and low content of this element. The material with medium silicon content has a higher hardness than the material with low silicon content near the periphery. The situation is reversed when approaching the core, with slightly higher hardness for the material with the lower silicon content.

The core region has the highest durability values in materials with a low and medium percentage of silicon. The zone has lower durability values in these materials but a lower standard deviation between measurements.

No high silicon cast iron has a homogeneity concerning durability values, which are close in regions with low standard deviation. In this material, the highest average durability occurred in the sample region.

4.2 Material characterization

The IMAGE PRO PLUS image software analyzed the mean sizes of graphite nodules, nodule shape, and mean percentage values of graphite in the pearlitic matrix. The results are shown in Table 6.

In general, the distribution of the types of graphite in the regions, considering the three types of materials, is shown in Figure 8, which is the graphical representation of Table 6. The figure shows the percentage per area of each type of graphite nodule found in the three regions of the three materials.

There is a higher percentage of spheroidal graphites for cast iron with high silicon in all three material regions. In addition to a more significant amount per area, the value of this type of graphite far exceeds the amounts of slightly irregular spheroidal graphite and irregular spheroidal graphite. In materials with medium and low silicon content, there is a more significant amount per area of slightly irregular spheroidal graphite in all regions, with higher values than the other two types, spheroidal and irregular spheroidal.

Materials with a more significant amount of spheroidal graphite have greater ductility than those with a predominance of graphite with some degree of irregularity. Another indication of the effect of silicon on carbon graphitization in cast iron is the higher percentage per area of formation of graphite nodules in general, which occurs in materials with higher silicon content (3.92 - 4.04%) compared to other materials with medium (3.06 – 3.08%) and low (2.52 – 2.54%) silicon.

4.3 Tool life

4.3.1 Cutting speed – 250 m/min

In the lower cutting speed condition, the average flank wear behavior of the cutting tool used in each region of the bar concerning the volume of material removed for the three materials tested is shown in Figure 9. The average flank wear (VB_B) is expressed in mm, and the volume removed is expressed in ($x10^3$ mm^3).

Table 5. Results of the Brinell hardness of the work materials

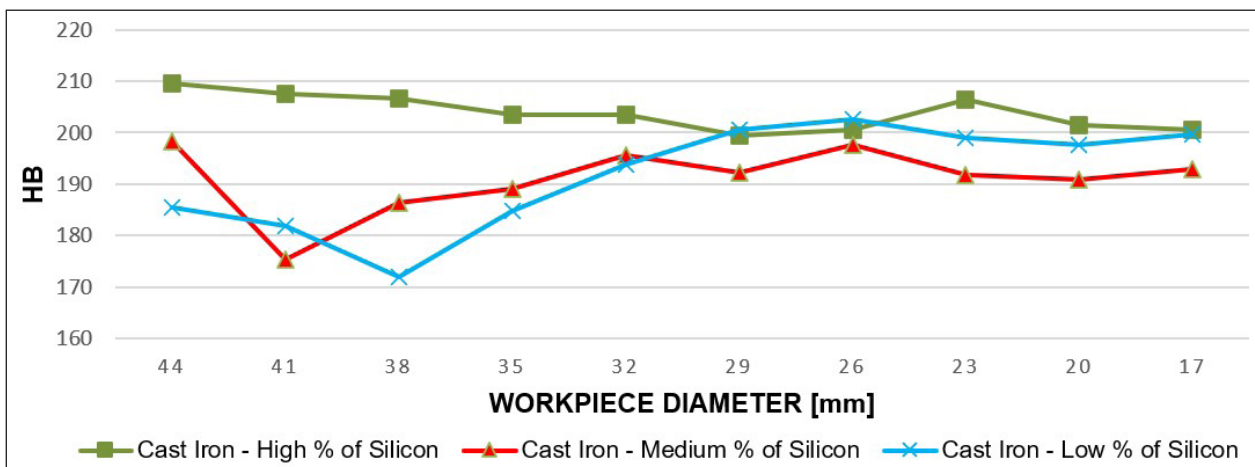| Materials	Regions	Average hardness [HB]	Standard Deviation [HB]
Low Si	Core	184	6
	Intermediate	179	6
	Periphery	183	4
Medium Si	Core	200	3
	Intermediate	187	3
	Periphery	176	3
High Si	Core	204	1
	Intermediate	206	1
	Periphery	205	2

Figure 7. Brinell hardness along the cross-section of the work materials.

Table 6. Average sizes of the graphite nodules of the three work materials according to their regions

| Types of Graphite	High Silicon						Medium Silicon						Low Silicon					
	Periphery		Intermediate		Core		Periphery		Intermediate		Core		Periphery		Intermediate		Core	
	Ø (μm)	% Area	Ø (μm)	% Area	Ø (μm)	% Area	Ø (μm)	% Area	Ø (μm)	% Area	Ø (μm)	% Area	Ø (μm)	% Area	Ø (μm)	% Area	Ø (μm)	% Area
Spheroidal Graphite	61.69	4.99	41.70	2.00	43.46	1.63	57.24	2.98	14.43	0.74	9.19	0.49	85.42	4.81	71.13	1.81	66.69	1.54
Slightly Irregular Spheroidal Graphite	68.30	1.49	156.43	2.86	192.92	3.09	90.25	2.40	182.03	2.42	189.92	2.09	128.40	2.90	260.07	3.96	250.84	2.82
Irregular Graphite	55.02	0.32	134.95	1.27	163.76	1.34	75.35	0.64	202.20	1.66	221.33	1.74	106.39	0.62	253.04	1.71	284.00	1.68
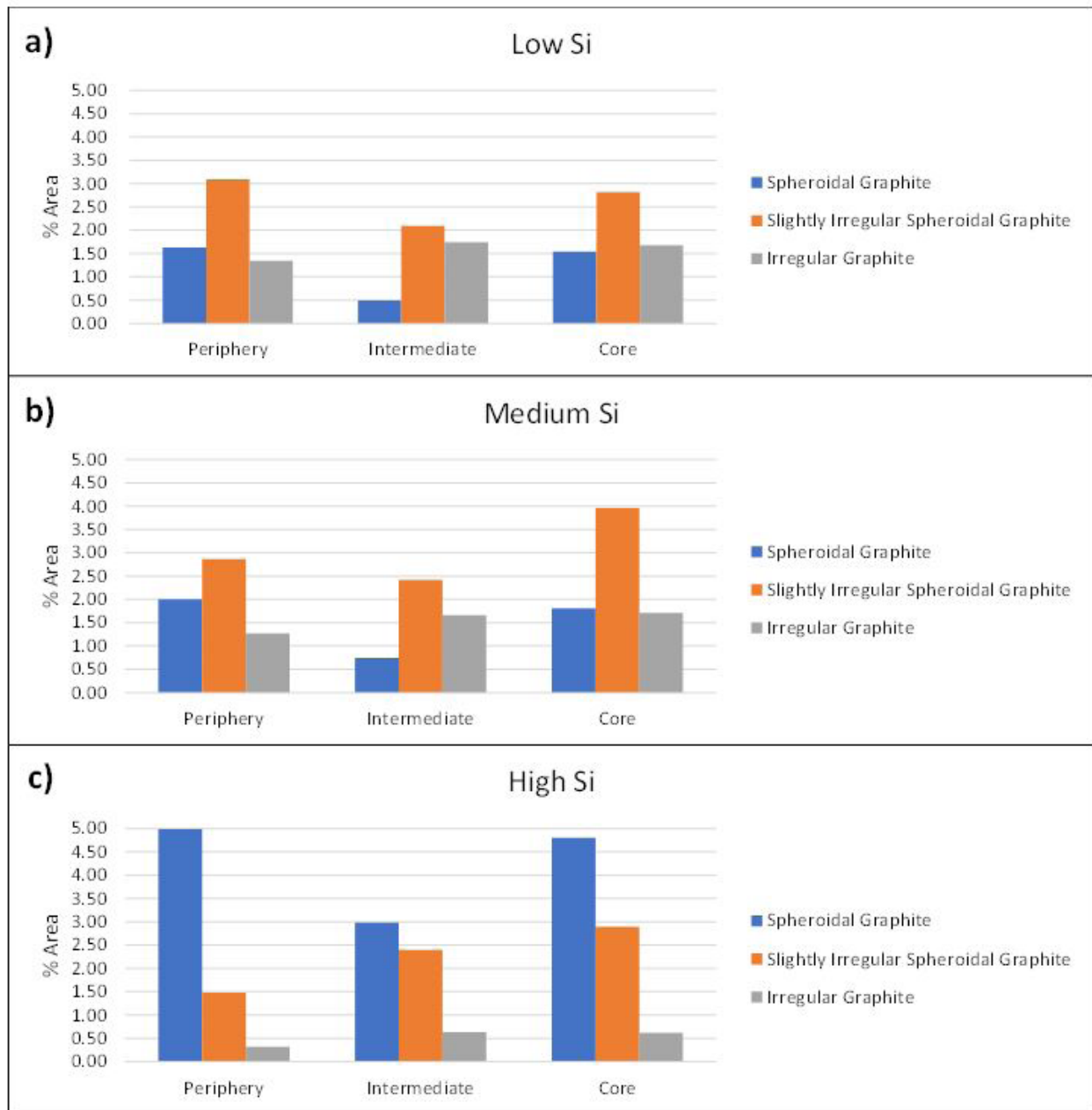
Figure 8. shows graphite nodules per region for the three work materials tested. (a) Low Si; (b) Medium Si; (c) High Si.
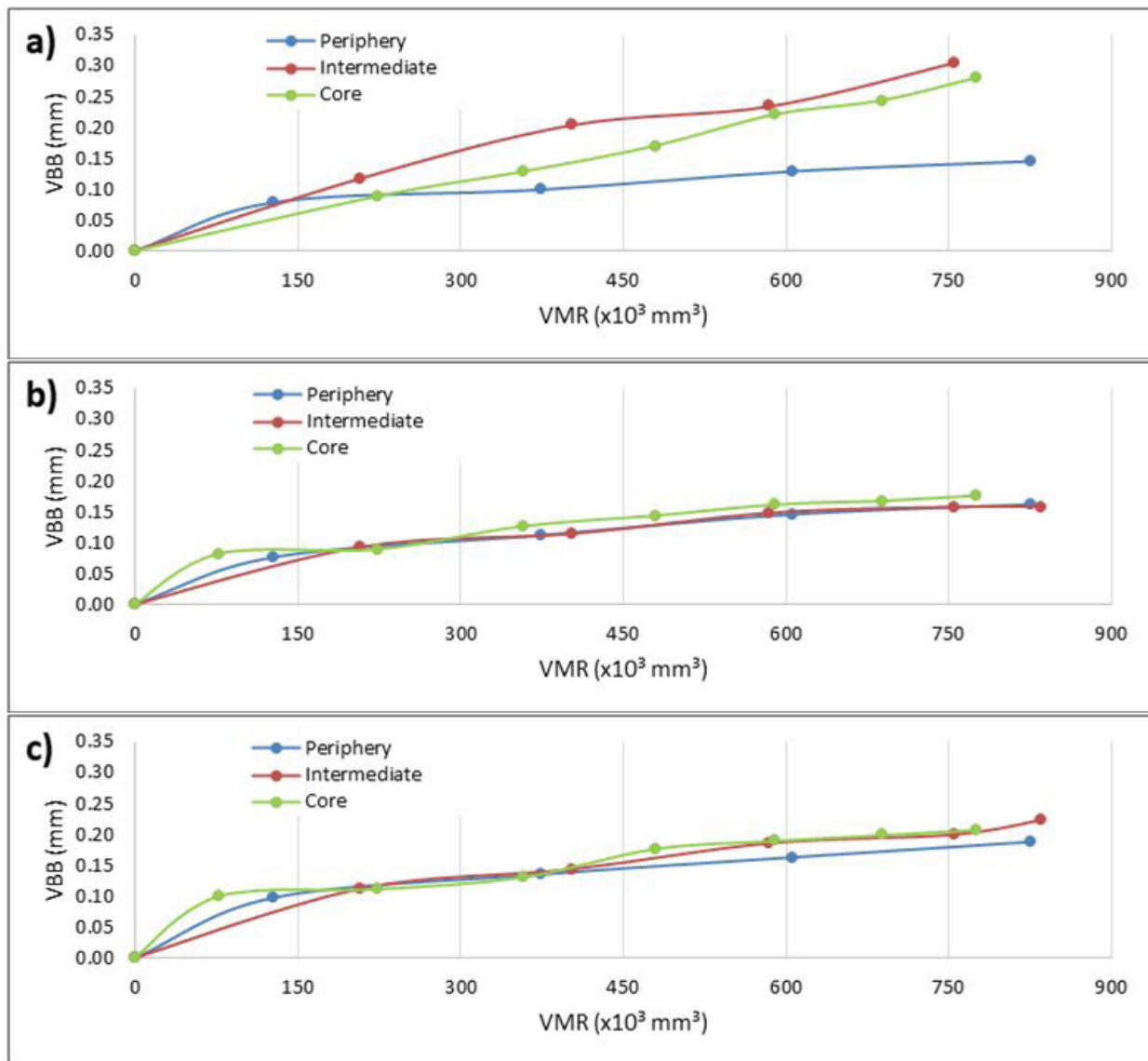
Figure 9. Average flank wear versus volume of material removed for the cutting speed of 250 m/min (f = 0,4 mm/rev and doc = 1 mm) for the three work materials tested, according to their regions. (a) Low Si; (b) Medium Si; (c) High Si.

The wear values presented for the three materials and their respective regions demonstrate that for materials with higher percentages of silicon, there is greater uniformity in the wear behavior of the tool between the regions when machined at a cutting speed of 250 m/min. The difference in the cutting tool life in material with low silicon was more significant between the regions, with higher values in the intermediate zone and the core of the sample.

Considering a removed material volume of 750 x 10^3 mm^3, there is a significant variation in the wear of the cutting tool on the periphery concerning the intermediate zone and core of the material with low silicon, with the last two getting closer. In the material with medium silicon, the tool life differences concerning the three regions are smaller, with the wear in the core region being more significant than in the other two regions.

In material with high silicon, the life behavior of the cutting tool is similar to that of material with medium silicon but with higher levels of wear throughout its tool life.

In the machining of low silicon cast iron, the differences in tool wear observed between the periphery and the other two regions are more than double, with an increase of 131% for the intermediate zone and 108% for the core, representing an essential difference in behavior between regions. The difference in wear between the intermediate zone and the core is approximately 10%, smaller in the intermediate zone. The size and spacing of graphite nodules and the amount of perlite directly influence this behavior. On the periphery, the nodules are considerably smaller with less space between them, and the amount of pearlite is smaller, ensuring greater machinability.

In material with medium silicon content, higher values of flank wear of the tool also occur as it approaches the central region of the material. The average wear in the periphery region in relation to the core was 20%, more significant in the core, considering the volume of 750×10^3 mm^3 of material removed. Comparing the periphery region with the intermediate zone, there was an increase in wear of 7%, and from this to the core, there was an increase of 13%.

For the material with high silicon content, the wear difference between the periphery and the core was approximately 25%, more significant in the latter. This level of wear is greater than that found in the material with medium silicon, where the difference in wear between the same regions was 20%. Considering the volume of 750×10^3 mm^3 of material removed, the wear levels of the tool from the periphery to the intermediate zone was 19%, and from this to the core was 5%.

The difference in wear levels was expected due to the variation in graphite percentage measured in each region. The spacing between the nodules, consequently the amount of perlite/ferrite, are variables noted in the metallography of the material and the photos of the regions shown in this work.

4.3.2 Cutting speed – 350 m/min

The average tool flank wear results concerning the volume of material removed for the highest cutting speed condition (350 m/min) are shown in Figure 10. Using the highest cutting speed of 350 m/min when machining low-silicon cast iron, the difference in wear levels between the periphery and the other two regions has been reduced. For a removed material volume of 750×10^3 mm^3, there was a reduction of 11% in the wear level of the periphery concerning the intermediate zone and an increase of 15% in

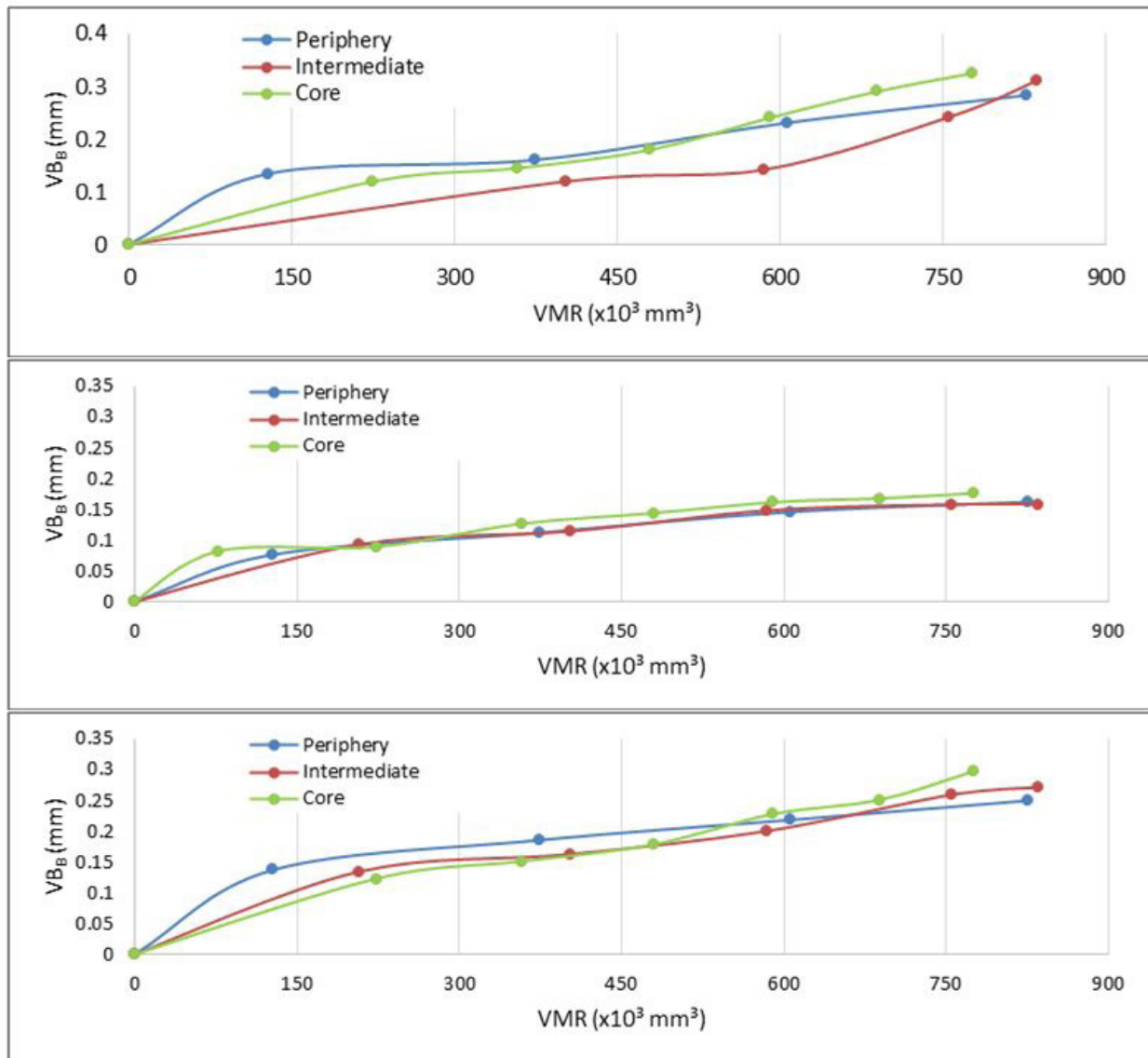**Figure 10.** Average flank wear versus volume of material removed for the cutting speed of 350 m/min (f = 0,4 mm/rev and doc = 1 mm) for the three work materials tested, according to their regions. (a) Low Si; (b) Medium Si; (c) High Si.

relation to the core. Comparing the core with the intermediate zone, the level of wear in the central region was 29% higher.

There were higher flank wear levels in the material with medium silicon content as the material's central region was advanced. The core showed 13% higher tool wear when compared to the periphery, with a lower variation than when used at a speed of 250 m/min. Comparing the wear level of the periphery with the intermediate zone, the wear in this second was 7% higher. The difference between the average flank wear in the intermediate region in relation to the core was 6%, higher in the core, considering the volume of 750 x 10^3 mm^3 of material removed.

For material with high silicon content, the difference in wear level between the periphery and the core was approximately 26%, being more significant in the latter. This level of wear is greater than that found in the material with medium silicon, where the difference in wear between the same regions was 13%. Considering the volume of removed material 750 x 10^3 mm^3, the increase in wear levels from the periphery to the intermediate zone was 13%, and from this to the core was 12%.

The more significant variation in hardness in the cross-section of the material with low silicon may explain the behavior of this material in relation to the others. Considering a removed material volume of 750 x 10^3 mm^3, the average flank wear level of the tools used in machining the three materials at the highest cutting speed was higher in the core, with

less difference than in the tests with a speed of 250 m /min. According to the classic machining literature (Ferraresi [16], Machado et al. [17], Trent and Wright [18]), the cutting speed directly affects the tool life, increasing the cutting speed and the machining temperature increases, resulting in a decrease in tool life. The influence of cutting speed depends on the type of material being machined, mainly on its strength and hardness. Therefore, selecting a suitable tool class depends on the cutting speed used for each material.

4.3.3 Roughness

The surface roughness parameter Ra was measured during turning in all regions of the three materials, in tool life tests carried out with cutting speeds of 250 m/min and 350 m/min. The Ra values obtained during all life tests for each material and region, with cutting speeds of 250 m/min and 350 m/min, are shown in Tables 7 and 8. These are average values obtained over the entire tool life. Table 9 compares the mean roughness parameters Ra between regions for both cutting speeds. Since the tool did not reach its wear limit in the tests, tool wear did not result in significant variations in roughness.

It is observed that, in general, the roughness increases from the periphery to the core. Exceptions were for the low Si material, which presented greater roughness in the intermediate zone than in the core, for a speed of 250 m/min; and in the medium Si content material, which presented the

Table 7. Surface roughness (Ra) for 250 m/min cutting speed

Region	Low Si		Medium Si		High Si	
	Ra (µm)	Standard deviation	Ra (µm)	Standard deviation	Ra (µm)	Standard deviation
Periphery	5.56	0.097	5.41	0.088	5.29	0.059
Intermediate zone	6.06	0.496	5.53	0.214	5.56	0.115
Core	5.74	0.234	5.77	0.198	5.79	0.187

Table 8. Surface roughness (Ra) for 350 m/min cutting speed

Region	Low Si		Medium Si		High Si	
	Ra (µm)	Standard deviation	Ra (µm)	Standard deviation	Ra (µm)	Standard deviation
Periphery	5.26	0.403	5.44	0.015	3.78	0.743
Intermediate zone	5.42	0.388	5.63	0.176	5.43	0.119
Core	5.78	0.180	4.74	0.677	5.50	0.052

Table 9. Comparisons of the surface roughness (Ra) obtained during the tool life tests at 250 e 350 m/min

Material	Comparisons	250 m/min	350 m/min
		Change (%)	Change (%)
Low Si	Periphery → Intermediate zone	9%	3%
	Periphery → Core	3%	10%
	Intermediate zone → Core	-5%	7%
Medium Si	Periphery → Intermediate zone	2%	3%
	Periphery → Core	7%	-13%
	Intermediate zone → Corre	4%	-16%
High Si	Periphery → Intermediate zone	5%	44%
	Periphery → Core	10%	45%
	Intermediate zone → Core	4%	1%

lowest roughness in the core at a cutting speed of 350 m/min. At the speed of 250 m/min, the roughness values were very close for the three materials in the periphery and the core. The material with low Si content presented higher Ra values than the other two materials in the intermediate region. At a speed of 350 m/min, the material with medium silicon content showed higher levels of surface roughness in the periphery and the intermediate region, but in the core, the material with the highest roughness was the one with low Si content. The standard in the periphery and the intermediate zone was low; however, the material with medium Si content presented a high deviation in the core region (0.677 µm, which is the most significant standard deviation found in all tests).

The roughness behavior for the lowest cutting speed in material with high silicon was similar to that found in medium silicon, with a higher value in the core region and low standard deviation. This may have been due to the greater hardness of the material with high silicon in this region, where the lowest roughness values occurred, combined with lower vibration of the assembly due to the lower shaft rotation and greater rigidity of the sample due to the larger diameter of the bar on the periphery.

Benedetti et al. [19] concluded that longer solidification times and smaller spheroidal graphite fractions result in lower tensile strength and that increasing the mean diameter of graphite nodules increases the fatigue crack growth threshold, a feature found in the core of the samples. The study pointed out that the spacing between the graphite nodules is also essential to determine the characteristics related to the material's roughness.

Analysis of variance - ANOVA results for tool life (given in a volume of material removed) and for cutting roughness Ra obtained in the tests, with a reliability index of 95% and a significance level of 5%, are shown in Table 10. Values of p-value < 0.05 highlighted in red show that the variable significantly influences the Ra results obtained.

It is observed that the amount of silicon statistically significantly influences the tool life results (VRM). Its interactions (individually and together) with cutting speed and the part region also significantly influence tool life. The interaction of cutting speed with the part region also presents a statistically significant difference.

Table 10. Statistic influence (p-values) of the input variables on the tool life (VMR) and surface roughness (Ra)

Variable and interactions	VMR	Ra
	ρ-value	ρ-value
Si content	0.017795	0.000005
Vc	0.110979	0.000020
Region	0.469863	0.000096
Si content and Vc	0.014613	0.040592
Si contente and Region	0.004629	0.334750
Vc and Region	0.019547	0.000005
Si contente, Vc and Region	0.019875	0.000001

Outstanding cutting speed and radial position (region) of the studied variables did not show significant influences, demonstrated by p-values greater than 0.05. The cutting speed did not show a significant influence and was considered a surprise since this parameter is one of the most influential on tool life, to the point where the tool life equation (Taylor Equation) is expressed as a function of this variable [17]. One explanation for this result is the choice of relatively close values for the chosen maximum and minimum speeds, 250 and 350 m/min, with a difference of approximately 28.5%. A higher cutting speed level was not chosen because of excessive assembly vibration during testing, particularly on the smallest machined diameters. Despite the tendency to reduce tool life from the periphery to the core of the part, the differences were not significant. The results may have been influenced by the rigidity of the set during machining because at each pass to remove the material, the cross-section becomes thinner and with less resistance of the set.

The interaction between silicon content and radial position (region) was the only situation that did not show statistically significant influences on roughness. The other variables, alone or in interactions, showed statistical influences on the values found.

4.4 Machining forces

The force tests were carried out on the three materials and in the three regions under the same conditions for various levels of feed and cutting speed (four feeds and four cutting speeds, with a fixed depth of cut at 1.0 mm). Measurements were taken of the three force components (cutting force, Fc, feed force, Ff, and passive force, Fp). The results will be analyzed by the machining force Fu, which is the vector sum of the three components, and in these tests, there was no influence of tool wear. The results are expressed considering the average of all tests in each region and by material separately. Figure 11 shows the values of the machining force as a function of the variation in cutting speed for the four levels used for each region studied, without distinguishing the materials and feeds tested.

With the variation of the cutting speed, a reduction in the machining force in the periphery and the intermediate zone and an oscillation of the machining force in the core region were obtained. The highest values of the machining force were measured in the intermediate zone and the lowest in the periphery, except for the cutting speed of 50 m/min, where the smallest value of the machining force was at the core.

The periphery region generally showed lower hardness levels, contributing to these results. There is probably the formation of Built-Up Edge – BUE at the two lowest cutting speeds due to the low temperatures developed in the chip-tool contact region, but probably already close to the critical cutting speed, above which BUE disappears [17]. The presence of BUE tends to reduce the machining force, as it increases the rake angle and considerably reduces the
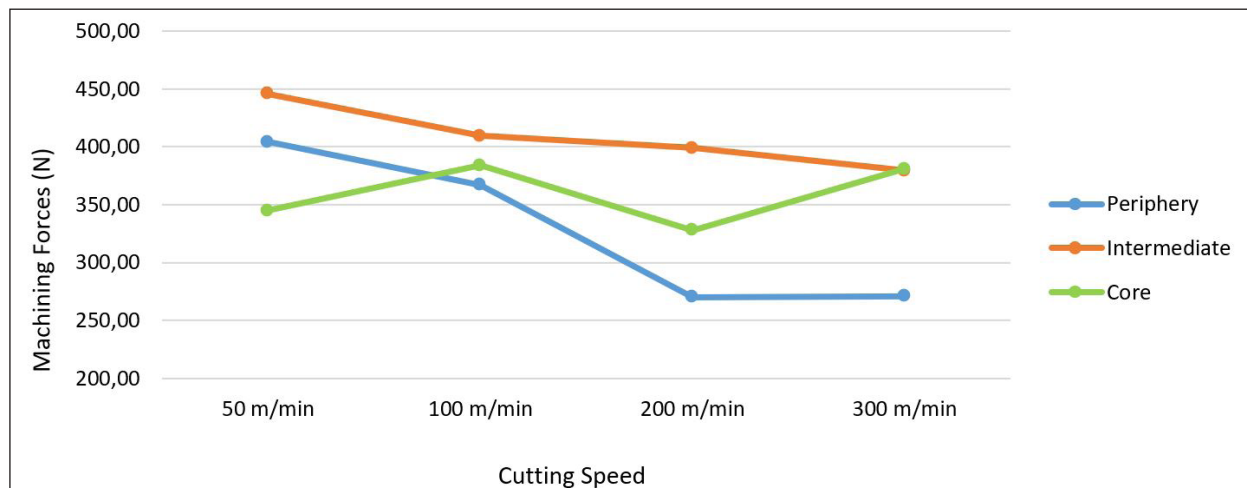
Figure 11. Machine force versus cutting speed according to the investigated cross-section regions (average of the three work materials)
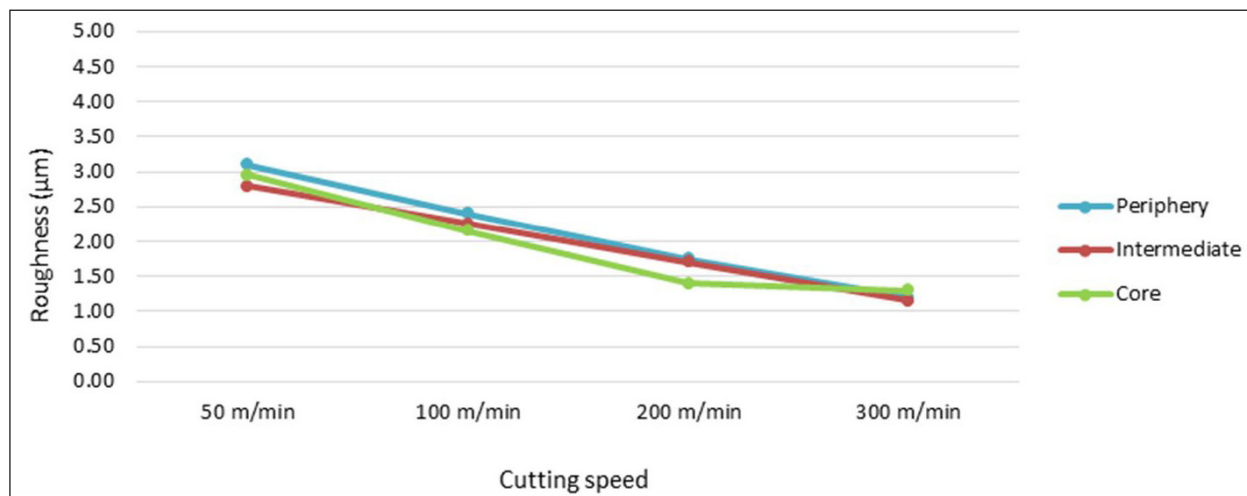

Figure 12. Surface roughness versus cutting speed according to the investigated cross-section regions (average of the three work materials).

length of the flux zone in the region of contact with the chip. This effect is more significant the more extensive the dimensions of the BUE.

At low cutting speeds, in addition to the tendency to form built-up cutting edge (BUE), less heat is generated and, therefore, lower temperatures are developed, causing higher machining forces. Conversely, temperature increases as cutting speed increases and, consequently, BUE decreases or disappears, and machining forces decrease. Parhad et al. [20], machining nodular cast iron, found in their experiments that the magnitude of the machining force components (Fx, Fy, and Fz) was maximum at the lowest cutting speed of 100 m/min, decreasing with increasing cutting speed to 200 m/min.

Another work that studied the influence of cutting speed on machining force was by Aslantas and Ucan [21], who concluded that in the machining of nodular cast iron, the increase in cutting speed promotes an increase in temperature even improving the quality of the machined surface. Şeker

and Hasirci [22] justify that, with the increase in cutting speed due to the increase in temperature, there is a reduction in shear forces, facilitating the removal of material by the shearing process. With the reduction of the machining force, gains are obtained with the reduction in the consumed power and the tool wear; therefore, the production rate is improved.

Figure 12 shows the roughness behavior as a function of cutting speed for the three regions investigated, considering the average found in machining the three materials in all feeds tested.

Roughness is also reduced with increasing cutting speed. The formation of BUE at low cutting speeds favors the development of a high roughness on the machined surface. It was probably present at the two lowest cutting speeds tested (50 and 100 m/min), disappearing at the highest speeds. Ghani et al. [23] verified that, for higher cutting speeds, the system tends to be more stable, as there is a reduction in forces, contributing to the reduction of roughness.

Figures 13 and 14 show the behavior of machining force and roughness of the machined surface as a feed (0.05; 0.10; 0.20 and 0.30 mm/rev) for the materials and regions studied. The results are expressed considering the average of materials by region, without distinction of material type and cutting speed used.

With the increase in feed, both the machining force and the roughness were obtained in all part regions. Increasing the feed increases the cutting section area, thus increasing the machining force [17]. The arithmetic means roughness is directly proportional to the square of the feed (Machado et al.) [17], thus justifying the behavior of the curves shown in Figure 13.

Increasing the feed increases the machining temperature, but the effect on tool life is much smaller than cutting speed. Although, according to Chang et al. [24], smaller feed increases tool wear for the same volume of material removed, as it increases cutting time.

With greater feed, therefore, better productivity is achieved.

The machining force remained higher in the periphery and intermediate zone of the materials in most of the tests, with the machining force in the core being smaller but with similar values. The intermediate zone may have shown this behavior because it presents a hardness close to the core, which is harder but has more remarkable tenacity since it has a smaller spacing of the graphite nodules. According to Guesser [1], in nodular cast iron with a ferritic matrix, fracture toughness increases with the number of graphite nodules.

Roughness increased with increasing advancement, as was to be expected. Souza and Silva [25] found results in the turning of nodular cast iron also showed the direct influence of advance on surface roughness when the smallest advance presented the best finishes. In these experiments, the advance was the most influential parameter in the surface roughness of the pieces among all the parameters studied. Werlang [26] concluded that the machinability would be
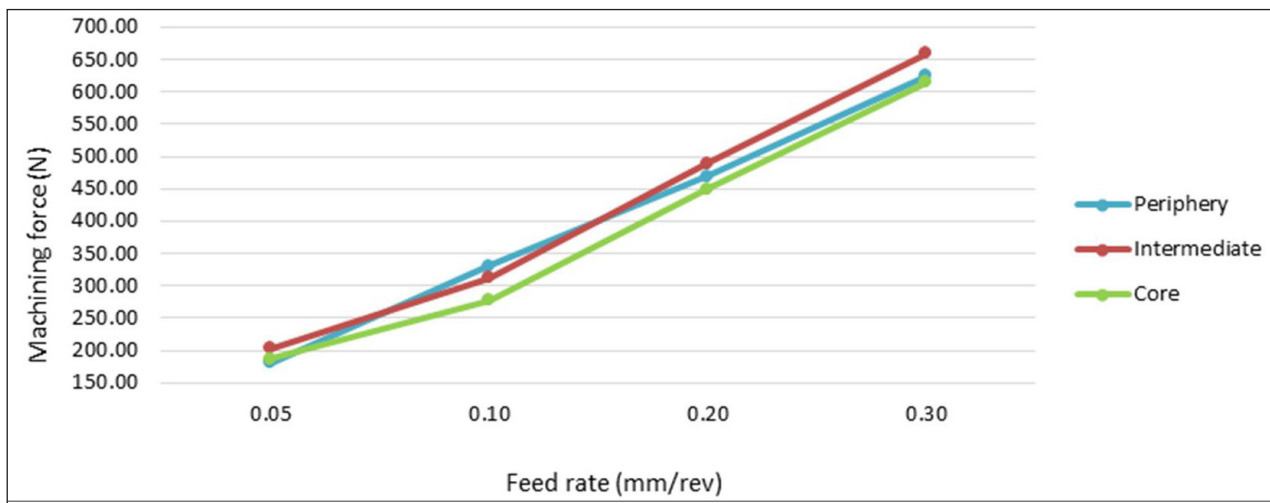

Figure 13. Machine force versus feed rate according to the investigated cross-section regions (average of the three work materials).
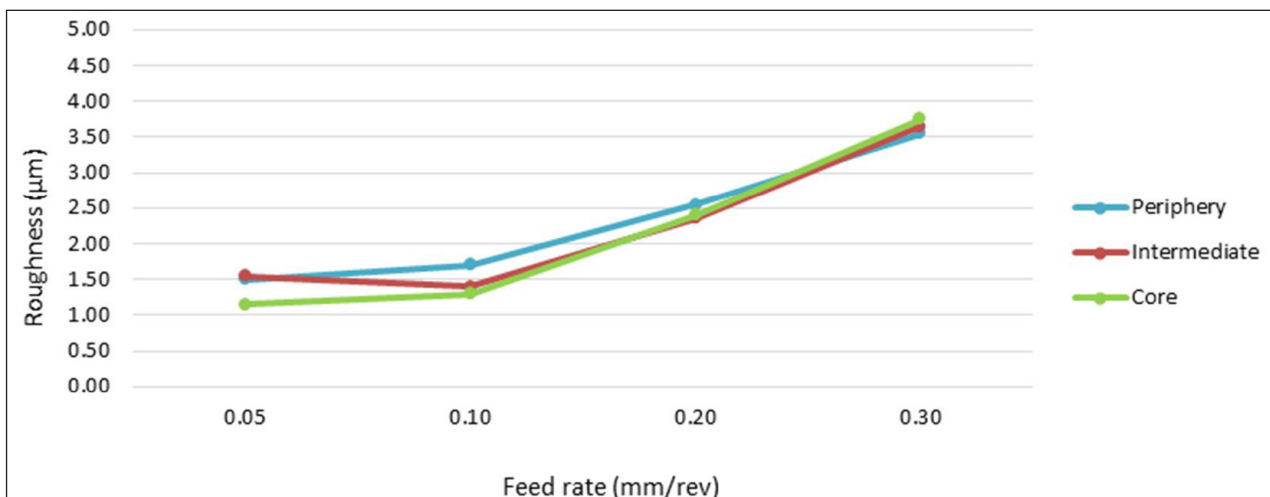

Figure 14. Surface roughness versus feed rate according to the investigated cross-section regions (average of the three work materials).

higher the lower the specific cutting pressure and the lower the cutting force. He also concluded that an increase in the depth of cut leads to greater cutting force and, consequently, a worse surface finish.

Table 11 shows the p-values after ANOVA, considering all strength and roughness results. For a reliability index of 95%, p-values < 0.05 indicate that the results obtained differ statistically. According to the results obtained, all variables (silicon content, radial position, cutting speed, and feed) and interactions significantly influence the machining force and part roughness, except for the "part and feed region" interaction which presented a p-value of 0.510 in the output variable "roughness," therefore, statistically not influential. However, this interaction would also be influential if the reliability index is reduced to 94.8%. The interaction of silicon content with cutting speed, region, and feed, also differs statistically, showing the significant influence of this variable on the results. Table 12 presents the values of

Table 11. Influence of the input variables on the cutting force and surface roughness

Variables	Cutting force p-value	Surface roughness p-value
Silicon content	0.0063	0.0218
Region	0.0286	0.0223
Cutting speed (Vc)	0.0324	0.0005
Feed rate (f)	0.0005	0.0002
Silicon contente * Region	0.0096	0.0093
Silicon content * Vc	0.0293	0.0206
Region * Vc	0.0208	0.0230
Silicon content * f	0.0066	0.0233
Region * f	0.0097	0.0510
Vc (m/min) * f (mm/rev)	0.0164	0.0086
Silicon contente * Region * Vc	0.0274	0.0148
Silicon content * Region * f	0.0040	0.0102
Silicon content * Vc * f	0.0188	0.0194
Region * Vc * f	0.0208	0.0160
Silicon content * Region * Vc * f	0.0105	0.0124

Table 12. Machining force [N] for all the three materials tested, according to their regions

Material	Region	VC (m/min)	f = 0.05	f = 0.1	f = 0.2	f = 0.3
High silicon 3.92 – 4.04% Si	Core	50	122	272	523	712
		100	182	316	517	658
		200	266	371	535	673
		300	241	327	471	614
	Intermediate zone	50	113	340	642	783
		100	191	329	520	709
		200	252	361	549	687
		300	238	326	484	626
	Periphery	50	146	385	671	829
		100	179	389	559	728
		200	267	354	524	668
		300	230	316	467	623
Medium silicon 3.05 – 3.08% Si	Core	50	75	189	417	614
		100	193	274	476	626
		200	185	285	448	543
		300	193	279	436	569
	Intermediate zone	50	119	314	552	705
		100	141	286	484	659
		200	153	249	437	590
		300	228	309	460	585
	Periphery	50	91	257	515	721
		100	184	345	546	709
		200	172	273	454	626
		300	229	311	474	601
Low silicon 2.52 – 2.54% Si	Core	50	76	181	420	617
		100	162	277	451	614
		200	191	189	274	591
		300	203	287	434	583
	Intermediate zone	50	92	298	569	727
		100	221	335	494	661
		200	238	310	476	627
		300	215	289	433	576
	Periphery	50	424	609	125	192
		100	315	796	145	1923
		200	96	121	159	190
		300	99	123	150	174

Machining Forces found for the three types of materials testing for all cutting conditions.

Considering a comparative analysis of the three materials, the highest machining forces were obtained for the high-silicon material in all three regions, periphery, intermediate, and core. This can be a consequence of the higher hardness of the material with high silicon in relation to the other two. There was a predominantly ferritic matrix in high silicon in the core and intermediate zone, with perlite veins in the peripheral area. In materials with low and medium silicon, the matrix on the periphery is similar to the matrix on the periphery of high silicon, but in the intermediate zone and the core, the matrix is ferritic/pearlitic.

The values obtained in the tests show that the material with low silicon content shows significant differences compared to the three regions of the sample, which is undesirable due to the change in behavior during machining relative to parameters defined for the cutting conditions. When comparing the same regions with the same machining parameters, medium and high silicon showed greater uniformity in all situations. The differences between the machining forces in the periphery, intermediate zone, and core were smaller when compared to each other, indicating that silicon helps reduce the differences in behavior between the regions of the material. However, the machining force values significantly increased with the high silicon content, providing greater tool wear and shorter life. The graphitizing effect of silicon can explain this.

The material with medium silicon in the composition presented a good uniformity of the machining force between the material regions under the same conditions but in a lower range of values than the material with high silicon. Thus, it can be concluded that silicon is essential for the nodularization of graphite during the alloy solidification process and that higher silicon values in the composition promote greater uniformity in the behavior of the machining force between the peripheral region and the core region, even though there are still differences in matrix type, size, and spacing of graphite nodules. Table 13 presents the values

Table 13. Surface roughness Ra [μm] for all the three materials tested, according to their regions

Material	Region	VC (m/min)	f = 0.05	f = 0.1	f = 0.2	f = 0.3
High silicon	**Core**	**50**	2.20	2.10	3.00	5.00
3.92 - 4.04% Si		**100**	1.20	1.40	2.80	3.80
		200	1.10	1.20	2.20	3.80
		300	0.70	0.90	1.80	4.00
	Intermediate zone	**50**	2.70	2.10	3.40	4.80
		100	1.80	1.60	2.50	3.80
		200	1.30	1.20	2.20	3.60
		300	0.60	0.70	1.60	3.60
	Periferia	**50**	2.30	2.30	3.40	5.00
		100	1.10	1.80	2.10	3.00
		200	1.30	1.30	1.90	3.00
		300	0.80	0.70	1.40	2.90
Medium silicon	**Core**	**50**	2.30	2.30	3.10	3.50
3.05 - 3.08% Si		**100**	1.90	1.80	3.00	4.40
		200	0.80	1.00	1.60	3.50
		300	0.70	0.80	1.70	3.70
	Intermediate zone	**50**	2.30	2.40	2.90	4.20
		100	1.90	1.80	2.70	3.20
		200	1.00	1.20	2.10	2.50
		300	0.70	0.80	1.70	2.80
	Periphery	**50**	2.90	3.10	3.80	5.10
		100	2.40	2.20	3.00	3.50
		200	1.40	1.40	2.70	3.70
		300	1.00	0.90	1.80	3.50
Low silicon	**Core**	**50**	2.90	2.50	3.20	3.80
2.52 - 2.54% Si		**100**	1.60	1.60	2.60	2.40
		200	0.80	1.00	2.00	3.00
		300	0.60	0.70	1.80	3.30
	Intermediate zone	**50**	2.30	2.20	3.90	5.00
		100	2.00	1.60	2.60	3.70
		200	1.00	1.10	2.20	4.00
		300	0.70	0.80	1.30	3.10
	Periphery	**50**	2.80	2.50	3.10	4.60
		100	2.30	2.40	2.70	3.60
		200	1.60	1.60	2.40	4.10
		300	1.00	0.80	1.50	3.30

of the roughness parameter Ra for the three materials tested in all machining conditions.

As mentioned, the roughness increased with the increase in feed, as expected, since the square of the feed influences the theoretical roughness. Regarding the results of roughness between the regions of the materials, it is observed that the effect of the microstructure formed during solidification, generating smaller and less spaced graphite nodules in the periphery region, unlike the core, with larger and more graphite nodules spaced, with the presence of ferrite and pearlite between them.

Bhople et al. [27], in machining austempered nodular cast iron, concluded that feed rate significantly affected cutting force and the interaction between feed and depth of cut. However, cutting speed was considered negligible in the main cutting force. Concerning roughness, the author concludes that the cutting speed showed the most significant influence on Ra. Furthermore, the interactions between cutting speed and feed also significantly influenced surface roughness.

5 Conclusions

The results found in the present investigation allow the following conclusions to be drawn.

- The silicon content affects the material's microstructure, which, together with the cooling rate, favors the differentiation of graphite nodules in different sizes, arrangements, and spacing. This differentiation contributes to the difference in the material's behavior in machining between regions along the cross-section;

- The greater the percentage of silicon, the greater the material's hardness. With greater hardness, there was the development of greater machining forces needed to shear the material. Even with different percentages of silicon, the variation in behavior along the cross-section still exists;

- The material with high silicon presented the highest machining forces in the tests carried out, both for the variation of the cutting speed and the feed's variation. This material had the worst machinability of the three in terms of cutting force, with an average roughness close to the other two materials;

- Cast iron with medium silicon content presented lower machining force and roughness values but close to high silicon. As with high-silicon cast iron, forces remained at a more stabilized level, without significant variations between regions of the material. Roughness remained at the same level as in other leagues. The life tests presented the lowest tool wear indices compared to other alloys in the same condition;

- However, the material with low silicon had the lowest hardness indices among the three materials, with a big difference between the regions. The region with the lowest hardness of material a was the periphery, which had the lowest machining force indices, but in most tests, it had the highest roughness compared to other alloys under the same test conditions. The differences in behavior between the three regions of the material with low silicon were the greatest found, affirming that the problem of machinability variability along the cross-section remains in this material;

- Even with lower machining force indices, the material with low silicon showed tool wear at levels similar to that of high silicon, which has a greater hardness in all regions analyzed. This can be considered bad from the standpoint of machinability, as the same wear for a less hard material indicates that other variables in the process need to be controlled;

- The medium-silicon material had the best machinability homogeneity indexes along the cross-section, showing that the silicon percentage of this material makes it with similar characteristics between regions, presenting more uniform responses to manufacturing requests.

References

1 Guesser WL. Propriedades mecânicas dos ferros fundidos. São Paulo: Editora Blucher; 2009.

2 Pacha-Gołębiowska H, Piekarska W. Mechanical properties of ductile cast iron relation to the charge elements. IOP Conference Series. Materials Science and Engineering. 2021;1199(1):012022.

3 Gorka A, Doru MS, Beñat B, Edurne A, Ramon S. Effect of tellurium on the nucleation process of spheroidal graphite in cast iron. Journal of Materials Research and Technology. 2022;19:4451-4462.

4 Tewary U, Paul D, Mehtani HK, Bhagavath S, Alankar A, Mohapatra G, et al. The origin of graphite morphology in cast iron. Acta Materialia. 2022;226:117660.

5   TUPY. Perfis de fundição contínua. FUCO Manual Técnico. Joinville: Indústria de Fundição Tupy; 1998.

6   Angelo ECA Jr. Caracterização de ferro fundido nodular obtido por fundição contínua [dissertação]. Curitiba: Programa de Pós-graduação em Engenharia Mecânica, Pontifícia Universidade Católica do Paraná; 2003.

7   Sousa JAG. Influência da microestrutura na usinabilidade do ferro fundido nodular FE45012 em diferentes bitolas, obtidos por fundição contínua [tese]. Uberlândia: Programa de Pós-graduação em Engenharia Mecânica, Universidade Federal de Uberlândia; 2014.

8   Stan I, Anca D, Stan S, Riposan I. Solidification pattern of si-alloyed, inoculated ductile cast irons, evaluated by thermal analysis. Metals. 2021;11(5):846.

9   Vilela F. Efeito de algumas variáveis de processo na obtenção de ferro fundido nodular ferrítico no estado bruto de fundição [mestrado]. São Caetano do Sul: Centro Universitário do Instituto Mauá de Tecnologia; 2010.

10 Arshad W, Mehmood A, Hashmi M, Rauf O. The effect of increasing silicon on mechanical properties of ductile iron. Journal of Physics: Conference Series. 2018;1082:1082.

11 Martins MC. Análise da usinabilidade na furação de ferros fundidos nodulares produzidos por fundição contínua. [dissertação]. Florianópolis: Programa de Pós-graduação em Engenharia Mecânica, Centro Tecnológico, Universidade Federal de Santa Catarina; 2018.

12 TUPY. Catálogo Técnico – CT 0614 – FUCO Perfis Fundidos. [cited 2020 Oct 20]. 2012. Available at: http://www.tupy.com.br

13 Sousa JAG. Influência da microestrutura na usinabilidade do ferro fundido nodular FE45012 em diferentes bitolas, obtidos por fundição contínua [tese]. Uberlândia: Programa de Pós-graduação em Engenharia Mecânica, Universidade Federal de Uberlândia; 2014.

14 PACE Technologies. Introduction to metallography [cited 2020 Oct 20]. 2012. Available at: https://www.metallographic.com/Brochures/Met-manual-2b.pdf

15 Tan E, Ögel B. Influence of heat treatment on the mechanical properties of AA6066 alloy. Turkish Journal of Engineering and Environmental Sciences. 2007;31(1):53-60.

16 Ferraresi D. Fundamentos da usinagem dos materiais, São Paulo: Ed Edgard Blucher Ltda; 1977. 751 p.

17 Machado AR, Abrão AM, Coelho RT, Silva MB. Teoria da usinagem dos materiais. 3. ed. São Paulo: Editora Edgard Blucher; 2015.

18 Trent EM, Wright PK. Metal cuttin. 4th ed. UK: Ed. Butterworths; 2000.

19 Benedetti M, Fontanari V, Lusuardi D. Effect of graphite morphology on the fatigue and fracture resistance of ferritic ductile cast iron. Engineering Fracture Mechanics. 2019;206:427-441.

20 Parhad P, Dakre V, Likhite A, Bhatt J. The impact of cutting speed and depth of cut on cutting force during turning of austempered ductile iron. Materials Today: Proceedings. 2019;19:663-669.

21 Aslantas K, Ucun I. The performance of ceramic and cermet cutting tools for the machining of austempered ductile iron. International Journal of Advanced Manufacturing Technology. 2009;41(7-8):642-650.

22 Şeker U, Hasirci H. Evaluation of machinability of austempered ductile irons in terms of cutting forces and surface quality. Journal of Materials Processing Technology. 2006;173(3):260-268.

23 Ghani AK, Choudhury IA, Husni. Study of tool life, surface roughness and vibration in machining nodular cast iron with ceramic tool. Journal of Materials Processing Technology. 2002;127(1):17-22.

24 Chang GW, Wang H, Yue X, Zhang H. Research of the feeding speed adopting cored-wire method to spheroidize ductile iron melt. Acta Metallurgica Sinica. English Letters. 2008;21(5):362-368.

25 Souza DCS, Silva ER. Contribuição ao estudo da influência dos parâmetros de core e da geometria da ferramenta na rugosidade superficial de peças torneadas. Goiás: URV; 2008.

26 Werlang A Fo. Análise da usinabilidade de ferros fundidos nodulares austemperados como função dos tratamentos térmicos e microestruturas [tese]. Porto Alegre: Programa de Pós-graduação em Engenharia e Tecnologia de Materiais, Pontifícia Universidade Católica do Rio Grande do Sul; 2015.

27 Bhople N, Patil N, Mastud S. The experimental investigations into dry turning of austempered ductile iron. Procedia Manufacturing. 2018;20:227-232.